ELSEVIER

Journal of Atmospheric and Solar-Terrestrial Physics 66 (2004) 1399–1409

Journal of ATMOSPHERIC AND SOLAR-TERRESTRIAL PHYSICS

www.elsevier.com/locate/jastp

Probing the solar wind-inner magnetospheric coupling: validation of relativistic electron flux models

D. Vassiliadis[a,*], R.S. Weigel[a], D.N. Baker[b], S.G. Kanekal[c], A.J. Klimas[d]

[a]*USRA at NASA/Goddard Space Flight Center, Greenbelt, MD 20850, USA*
[b]*Laboratory for Atmospheric and Space Physics, University of Colorado, Boulder, CO 80309, USA*
[c]*Department of Physics, Catholic University of America, Washington, DC 20064, USA*
[d]*Laboratory for Extraterrestrial Physics, NASA/Goddard Space Flight Center, Greenbelt, MD 20771, USA*

Received 3 February 2004; received in revised form 23 March 2004; accepted 25 March 2004

Abstract

High fluxes of relativistic electrons in the inner magnetosphere have been associated with a range of spacecraft anomalies, and therefore the modeling of the flux is of direct relevance to the development of space weather applications. Time variations of the electron flux at a given L shell are ultimately functions of interplanetary parameters as well as of internal magnetospheric dynamics. It is important to resolve which one of the two elements is important for modeling and to what extent. To that end we compare two models of the magnetospheric relativistic electron flux at 2–6 MeV spanning the range $L = 1$–10 and driven by the solar wind plasma velocity, V_{SW}. The finite-impulse-response (FIR) model represents the coupling of the flux to the solar wind velocity. It is part of an empirical model chain currently in development at the Center for Integrated Space Weather Modeling. The autoregressive moving-average (ARMA) model also includes a representation of the internal flux dynamics. The comparison is quantified in terms of the prediction accuracy, its variation with season and solar cycle phase, and its dependence on activity level. We find that the FIR model is more accurate than the ARMA model in most radial regions of the radiation belts, including the geosynchronous orbit. The results indicate that the long memory of the FIR model to past solar wind velocity inputs is more important in representing the effective coupling than ARMA's additional internal dynamics.

Keywords: Magnetic storms; Solar wind/magnetosphere interactions; Radiation belts; Particle acceleration; Solar cycle; Forecasting; Space weather

1. Introduction

Intensifications of the magnetospheric relativistic electron flux are an important component of space weather (Behnke et al., 1997). High fluxes of relativistic electrons may produce damages or even failures on spacecraft, typically through surface or internal electrostatic discharges (Koons et al., 1999). Forecasting of this and other space weather components is therefore of importance to the satellite industry and other spacecraft service users. The Center for Integrated Space Weather Modeling (CISM) is a new institute with the mission of developing a comprehensive space weather forecasting model, in coordination with government agencies and the user communities (Baker et al., 2004).

*Corresponding author. Tel.: +1-301-286-9060; fax: +1-301-286-1433.
E-mail address: Vassi@electra.gsfc.nasa.gov (D. Vassiliadis).

1364-6826/$ - see front matter © 2004 Published by Elsevier Ltd.
doi:10.1016/j.jastp.2004.03.025

We have developed predictive models for the time variations of the relativistic electron flux and this paper discusses the validation of two such models. Model validation is an integral part of model development for space weather applications (Doggett, 1996). At the same time we can draw valuable conclusions for the physically correct representation of the solar wind–magnetosphere coupling. Both models represent the effective coupling of the electron flux to the solar wind plasma velocity in the radial direction, the single most important interplanetary parameter for the flux dynamics. The coupling to interplanetary parameters is particularly important during the passage of solar wind structures from 1 AU, such as high-speed streams, CMEs, and interplanetary shocks (e.g., Paulikas and Blake, 1979; Blake et al., 1997; Baker et al., 1998; Reeves et al., 1998).

Earlier analysis and modeling has shown that the response of trapped relativistic electrons depends significantly on the L shell. The correlation function of the flux time histories shows that there are three regions in the outer belt with distinct dynamics (Vassiliadis et al., 2003b). The flux in each region is preceded by different combinations of solar wind and IMF precursors (Vassiliadis et al., 2003a), while the response of the flux to the solar wind velocity (Vassiliadis et al., 2002 (hereafter: V2002)) and other variables (Vassiliadis et al., 2004) is different for each region.

This mapping of the outer belt in terms of the L parameter will be used in this paper in the interpretation of the validation results, so we briefly review it below:

- The P_1 region, at $L = 4.0$–7.5, is the region most closely to what is traditionally termed the "heart of the outer zone". It is characterized by high fluxes, long-term trapping, and a response which peaks 2–3 days after the arrival at the magnetopause of geoeffective solar wind structures, typically high-speed streams. It includes the flux variations at geosynchronous orbit, which have a well-known response to the solar wind plasma velocity (Paulikas and Blake, 1979). The most geoeffective structures for P_1 are high-speed streams.
- The P_0 region, at $L = 3.0$–4.0, is the inside edge of the outer belt. Its fluxes are comparable to, but lower than, those of P_1. Its response is drastically different, starting several hours (<1 day) after the solar wind arrival. Several case studies have shown that CMEs are the most geoeffective solar wind structures for P_0 (Baker et al., 1998; Reeves et al., 1998).
- Beyond P_1, the P_2 region overlaps with the inner plasma sheet. It is characterized by transient, low-amplitude fluxes. It has a brief (~ 1 day) response to solar wind and IMF variations, but in many respects this response is opposite from the response in P_1 (Vassiliadis et al., 2003a). In terms of a characteristic type of solar wind/IMF input, Northward B_z is the most representative condition preceding increased fluxes in P_2.
- In addition to those regions we will refer to the slot region (S) at $L = 2.0$–3.0 and the inner belt (IB) at $L = 1.0$–2.0. These have lower fluxes than the outer belt and very different responses to the solar wind speed (V2002) and other parameters (Vassiliadis et al., 2004).

2. The models

Both models are representations of the time variation of the logarithm base-10 flux, where the flux is measured in $\#/cm^2/sr/s$. This "log-flux" $j_e(t; L; E)$ is expressed as a function of time t, L parameter, and energy range E_0. Directional flux measurements at $E_0 = 2$–6 MeV have been taken by the Proton–Electron Telescope (PET) (Cook et al., 1993) on the Solar, Anomalous, and Magnetospheric Particle Explorer (SAMPEX). Here we will examine the flux at distances $L = 1$–10, where the L parameter has been calculated from the IGRF magnetic field model. The usefulness and certain limitations of the SAMPEX/PET directional flux dataset are discussed in V2002. The resolution in L is $\delta L = 0.1$ and the measurements are time-averaged to a daily resolution.

Flux variations in the radiation belts are ultimately determined by the conditions in the interplanetary medium and the magnetosphere (e.g., Fung et al., 2004). It is generally accepted that the single most important interplanetary parameter determining the relativistic electron flux in the geosynchronous region and elsewhere is the solar wind plasma speed, $V_{SW}(t)$. Increases in the speed excite fluid instabilities at the magnetosphere's dayside and flanks (Farrugia et al., 2001) which in turn lead to growth of ULF waves (Rostoker et al., 1998; Hudson et al., 1999). Wave-particle interaction is one of the dominant mechanisms for production of relativistic electrons (Friedel et al., 2002). Measurements of V_{SW} typically come from spacecraft at the libration point L_1 far upstream of Earth. Since, however, the resolution time is long compared to the propagation time to Earth, the measuring spacecraft can be anywhere in the region between L_1 and the dayside magnetopause.

The models are representations of the time variations of the flux due to its effective coupling with the solar wind speed. Ideally this coupling would be modeled with a global magnetospheric model endowed with kinetic effects in the ring current region and elsewhere. Current simulation capabilities, however, make such a modeling approach unfeasible. Hence the

empirical FIR and ARMA models provide a way to represent and forecast the effects of the coupling. Secondary geoeffective solar wind or IMF parameters such as the IMF B_z coupling are ignored in these single-input models, and are discussed elsewhere (Vassiliadis et al., 2004).

2.1. The FIR model

The flux level at a given L shell on a particular day t is the result of a number of processes driven and/or modulated by V_{SW}. Some of them have been outlined above. The timescales of the processes vary from several hours to several days, and therefore the log-flux $j_e(t;L)$ at time t is the cumulative effect of all such processes. The finite-impulse-response (FIR) model is the approximation that j_e responds linearly to the weighted time average of the recent solar wind speed.

$$j_e(t;L) = \int_{-T_s}^{T} H(\tau;L) V_{SW}(t-\tau)\,\mathrm{d}\tau. \quad (1)$$

The impulse response function $H(\tau;L)$ is parametrized by the L parameter. We set the timescale T to 20 days (V2002), but have also measured the response with $T=4$ and 8 days to compare with the shorter-memory ARMA model. Ideally T_s is 0, but in order to increase the signal to noise ratio in the impulse response function we set $T_s = 10$ days.

In particular, the FIR model for the geosynchronous orbit, $L = 6.6$, is identical to an earlier model developed for that region (Baker et al., 1990). The main features of $H(\tau; L=6.6)$ are a peak at $\tau = 2$–3 days which represents the net effect of acceleration processes related to V_{SW}; a subsequent decay which lasts 6 days, and a minimum at $\tau = 0$ corresponding to the temporary displacement of electrons due to the quasiadiabatic effects of the ring current. These effects have been discussed in detail elsewhere (Baker et al., 1990; V2002). The response to V_{SW} is qualitatively very similar in all L shells of the P_1 and P_2 regions, including the geosynchronous orbit.

2.2. The ARMA model

In addition to the external driving, time variations in the local log-flux $j_e(t; L = const.)$ may be due to internal acceleration processes (producing a growth in j_e), loss processes (decay), and adiabatic changes (oscillatory behavior). Flux transport from other L shells may produce some of these dynamic behavior as well. The autoregressive-moving average (ARMA) model represents such dynamics by relating $j_e(t)$ to earlier log-fluxes, up to m days in the past, as well as the interplanetary V_{SW} activity over the same days

$$j_e(t+1;L) = \sum_{i=0}^{m-1} a_i j_e(t-i\Delta t;L) + \sum_{j=0}^{l-1} b_j V_{SW}(t-j\Delta t). \quad (2)$$

We use $m = l = 4$ as standard settings, but we have also measured the response with $m = l = 8$. The coefficients a_i represent the flux's own dynamic effects, while b_j represent the effective coupling to V_{SW}.

The FIR and ARMA models are approximately equivalent (in the limit of the time resolution going to zero) if (a) the internal dynamics is negligible compared to the external driving, and (b) the memory time to variations of $V_{SW}(t)$ is comparable, i.e., here: $l = 4$ days or less. In other words, the equivalence is expected to occur during periods of strong, fast (compared to the timescale of model (1)) coupling to V_{SW}.

3. The validation procedure

Comparing the performance of the models helps evaluate the effect of a long memory time versus that of flux dynamics. We measure the model performance as a function of three variables:

- *L parameter*. The prediction accuracy is different for each of the two belts and the slot. Moreover, the regions P_i ($i = 0, 1, 2$) of the outer belt are differentiated by their responses as well.
- *Solar-cycle and seasonal phase*. The coupling of the magnetosphere to the solar wind varies quasi-regularly at these long timescales. In particular, seasonal variations of geomagnetic activity have been explained in terms of the IMF (Russell and McPherron, 1973) and solar wind velocity (Boller and Stolov, 1970) effects. Probably as a consequence of these and other variations in the coupling, there is a seasonal variation in the magnetospheric energetic electron flux (Baker et al., 1999).
- *Activity level*. In space weather forecasting, prediction of the highest disturbance amplitudes is most desirable. However, from a modeling standpoint it is also important to understand the model performance at lower activity levels. We therefore characterize each model's accuracy as a function of the activity level of the test interval.

3.1. Metrics

A number of validation methods have been developed to measure the performance of tropospheric and space weather forecasting models (Doggett, 1996). Here we will use two standard metrics to quantify the model

performance, one of which is a measure of the agreement of observations and model output in phase, while the other also includes the accuracy in amplitude.

- *Data-model correlation.*

$$C(L) = \frac{1}{T_{\text{test}}\sigma_{\hat{j}_e}\sigma_{j_e}} \sum_{t=1}^{T_{\text{test}}} (\hat{j}_e(t;L) - \langle \hat{j}_e \rangle)(j_e(t;L) - \langle j_e \rangle). \tag{3}$$

  Here $\hat{j}_e(t;L)$ is the model output and $j_e(t;L)$ is the observed log-flux, and $\sigma_{\hat{j}_e}$ and σ_{j_e} are their standard deviations. The correlation is computed over the length T_{test} of the test interval.

- *Normalized prediction error.*

$$e(L) = \frac{1}{T_{\text{test}}\sigma_{j_e}} \left[\sum_{t=1}^{T_{\text{test}}} (\hat{j}_e(t;L) - j_e(t;L))^2 \right]^{1/2}. \tag{4}$$

  We use this rms-type prediction error because the probability distribution of $j_e(t)$ is often reasonably close to Gaussian. If the distribution were heavy-tailed, a more robust statistic, such as the average absolute error, would be needed (Vassiliadis, 2000). The rms prediction error is related to the historical measure of "prediction efficiency", $\text{PE} = 1 - e^2$.

Using the above metrics we have examined test sets of several different lengths, from several days (individual events) to 1 year. Below we present primarily findings of analysis on 1-month intervals which are useful in determining the seasonal and solar-cycle variation of the prediction accuracy. The average monthly flux is used to measure the activity level as a function of L.

Note that the training set of the model is the entire dataset (1993–2001) of PET observations at energy range E_0 while the test sets are month-long intervals drawn from the same dataset, and therefore in principle the validation is in-sample (Vassiliadis and Klimas, 1996). However, because (a) the models are linear (as opposed to nonlinear or adaptive), and (b) the test sets are much shorter than the training set, each individual test set is not statistically significant in defining the model coefficients. Therefore in practice the validation procedure is out of sample, as it should be.

4. Results

Comparisons between the FIR and other models and SAMPEX measurements have been presented by Rigler et al. (2004). As an example for individual storm intervals, we focus on the performance of the FIR44 and ARMA models for the May 4, 1998 storm (Fig. 1). During that event, the passage of a complex interplanetary coronal mass ejection, composed of ejecta interacting with and overtaking a CME at 1 AU (Farrugia et al., 2003), produced a rapid acceleration of electrons in the radiation belts. The observed fluxes are shown in Fig. 1a. For comparison, the FIR model flux is shown in 1b, and the ARMA model flux in 1c. For both models, the predicted amplitudes are significantly lower than the observations, while the agreement in phase between predictions and observations is good.

We use the data-model correlation (4) to quantify the agreement between model and data as a function of L. Fig. 2a shows the $C(L)$ profile in the case of the May 1998 storm. The $C(L)$ corresponding to the FIR model is shown as the black curve and that of the ARMA

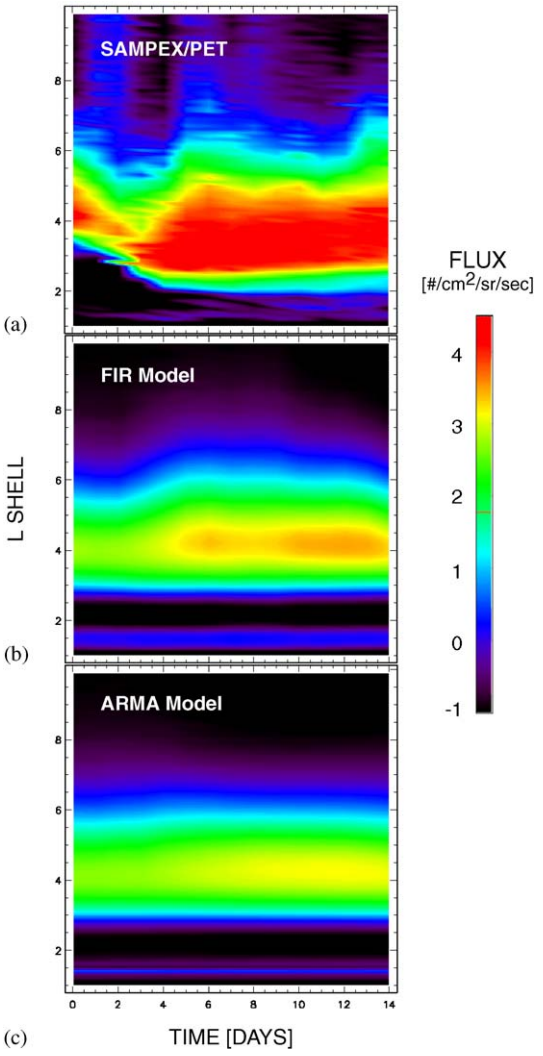

Fig. 1. Electron flux daily averages at $L = 1$–10 during the storm of May 4, 1998. (a) Observed. (b) Produced by the FIR model driven by the solar wind velocity, V_{SW}. (c) Produced by the ARMA model. Both predictions are lower in maximum flux amplitude than the observations. The relative phase difference between observations and model predictions is small.

model as the red curve. A horizontal dotted line denotes the correlation of 70% which would correspond to a prediction efficiency value of approximately $C^2(L) \sim 50\%$, provided the errors were not correlated with the activity level. The correlation reaches a maximum (>80%) at P_0 from which it steadily decreases as L increases in P_1. After a minimum near the geosynchronous region, $C(L)$ increases again in P_2 for both models. The correlation varies significantly in the slot and inner belt. Here the ARMA model has lower correlation values which shows that the average dynamic terms (coefficients a_i in (2)) do not represent the flux dynamics during individual storms. The $e(L)$ profile is in many respects a mirror image of the correlation profile.

Fig. 2b shows the same statistics, but from an analysis on an entire year of flux data (1998). The highest correlation is again at P_0. For higher L, the correlation for the FIR model decreases slowly with L in P_1 and P_2 (as in V2002). The correlation for the ARMA model, however, is lower and in fact negative in P_2, indicating again that the average dynamic terms do not represent the dynamics of the marginally trapped flux in P_2. Note that the prediction error has peaks near the S–P_0 boundary and the geosynchronous region. This suggests that the observed flux activity in those regions is determined by variables other than V_{SW} (namely ionospheric density and IMF B_{South}, respectively (Vassiliadis et al., 2004)).

As the test interval T_{test} increases, the data-model correlation decreases in absolute magnitude. If T_{test} spans a year (1998), the high-correlation range in P_0 and lower part of P_1 decreases to 40–50% from the 70–80% measured for a single storm. The decrease is a statistical effect: since the model is linear and the actual activity is not, a larger interval is more probable to contain instances where the model accuracy is lower.

There are several conclusions one may draw from this comparison:

(1) As expected, the solar wind velocity is a significant driver in producing the observed log-flux, especially in the central outer belt P_1 and somewhat less in its inside layer, P_0. The different responses characterizing regions P_0 and P_1 (V2002) are seen here as well. In these regions, the two models are approximately equivalent.
(2) For region P_2, the accuracy of the FIR model is higher than that of the ARMA model. This suggests that the coupling of the marginally-trapped flux to the solar wind velocity is represented better by a long-memory model than with a short-memory one, and internal dynamical terms are not necessary.
(3) Boundary layers: The V_{SW} can be used to explain the fluxes in P_0 and P_1, but it does not account for the flux variations in the S–P_0 boundary and the

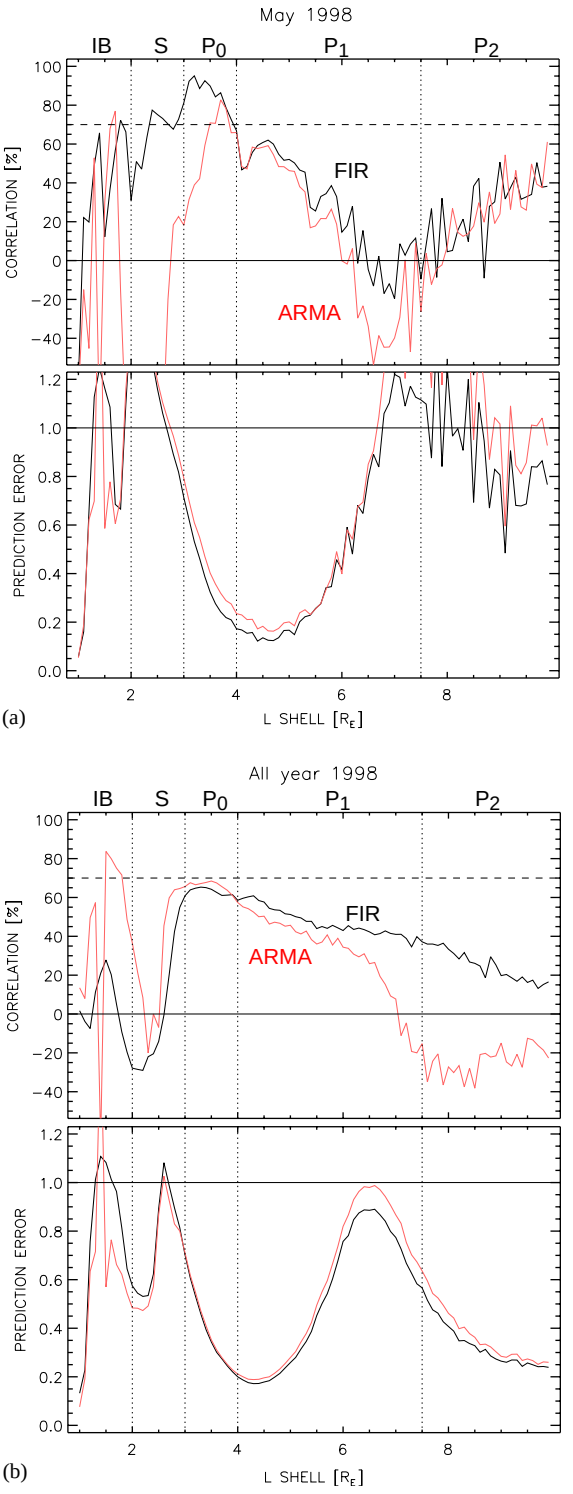

Fig. 2. The performance metrics of data-model correlation (4) and prediction error (5) for the May 1998 storm of Fig. 1. (b) Same for the entire year of 1998. Regions of the inner magnetosphere (IB, S, P*i*) are indicated at the top, with their boundaries defined by radial correlation analysis (Vassiliadis et al., 2003b).

geosynchronous region as well as it does in P_0 and P_1. A separate study shows that other solar/interplanetary inputs, and different physics, are important in those two boundary regions (Vassiliadis et al., 2004).

4.1. Solar-cycle variation

The variability of the input during a solar cycle gives important information for the scope of applicability of the model. We calculated $C(L)$ and $e(L)$ for monthly intervals in 1993–2001 and show the correlation $C(L)$ as a function of solar cycle in Figs. 3 and 4.

Figs. 3a and b share several similarities. For both models, vertical bands indicate high-V_{SW} intervals containing several types of geoeffective structures. During solar minimum (1995–1996) the 27-day periodicity of high-speed streams results in a similar periodic high correlation in the range $5<L<8$. For both models this period had the highest correlations compared to any other in the solar cycle. However, these high correlations occur over a narrower L range than during other solar cycle phases.

There are significant differences as well. While the FIR model performs well for a wide range of L, the ARMA model has a comparably high correlation only for $4<L<6.5$. For higher L values than 6.5, the ARMA model does poorly. In region P_2, therefore, the additional dynamical terms of the ARMA model are a liability rather than an asset.

A second, minor, difference is that at the peak of the solar minimum the ARMA model has distinctly higher correlations in the range $3.5<L<5$ than the FIR model. In all other times, the correlations are approximately equal.

The prediction-error profiles of both models are qualitatively very similar so only that of the FIR model is shown (Fig. 4). Only values of $e<1$ are included, since $e=1$ corresponds to the simple model $j_e(t;L)=\langle j_e(L)\rangle$. For both models the largest prediction errors occur close to $L=2.7$ and 6.6, namely close to the boundaries S–P_0 and P_1–P_2 mentioned above. However, the regions where the error is above 1 varies with the solar cycle. As we approach solar maximum, there is a decrease in the L range where $e(L)$ is low. For instance, for $e_{rms}<0.5$ the range decreases from $3<L<5.5$ to $3.5<L<5.0$.

Generally the FIR model is the more accurate of the two in the outer belt. The only times and L ranges where the ARMA model is more accurate are the following:

- The slot, especially during solar minimum.
- The inner belt, irrespective of solar cycle phase.
- Regions P_0 and P_2 during solar maximum.

Thus the additional oscillatory dynamics from terms $a_i j_e(t-i;L)$ become important during those times.

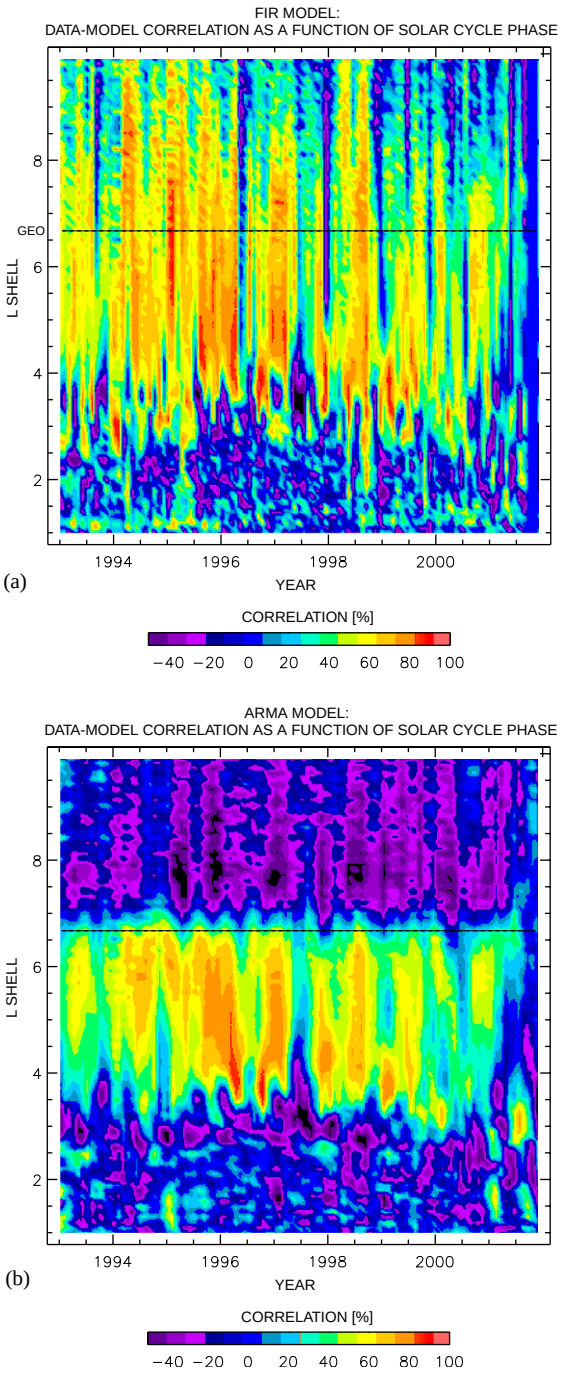

Fig. 3. Solar-cycle-phase variation of predictability. (a) The data-model correlation of the FIR model is shown as a function of time for 1993–2001. The test interval length is 1 month. (b) Same as (a) for the ARMA model. The geosynchronous orbit at $L=6.6$ is marked with a horizontal dashed line.

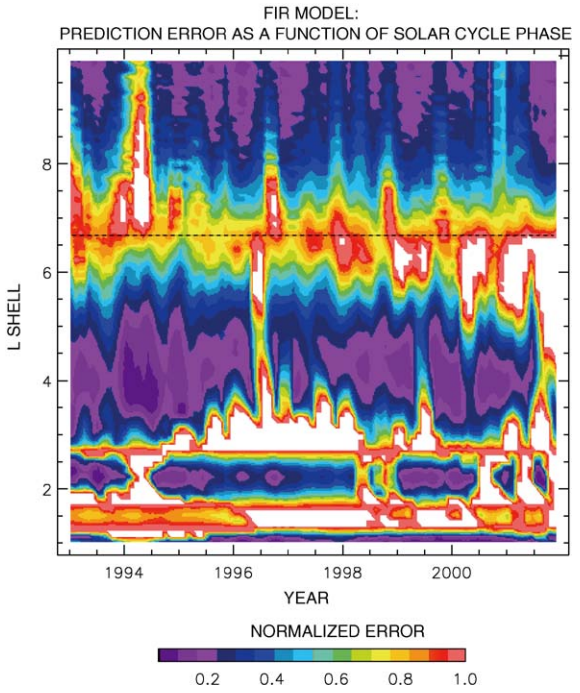

Fig. 4. Solar-cycle-phase variation: prediction error of the FIR model (cf. Fig. 3).

In order to make a more accurate comparison between the two models we have repeated the validation procedure with different timescales for the models as follows:

(a) Reduced the memory time of the FIR model to $T =$ 4 and 8 days (T_s was set to 0 days).
(b) Increased the number of terms in the ARMA model to $m = l = 8$ days.

Decreasing the memory time T reduces the accuracy of the FIR model. The 4th order FIR model is approximately as accurate in terms of prediction error as a 4th order ARMA model, but significantly less accurate than a 20th order FIR model. On the other hand, increasing the ARMA order tends to overfit its training data and also lead to a reduction in prediction accuracy. In summary, long memory times are best for the FIR model, and short-term dynamics give the best prediction results for the ARMA model.

Thus the conclusions from the solar-cycle variation of the predictability are the following:

(4) The FIR model is again the more accurate of the two in the outer belt. The ARMA model is an improvement only in specific times and mostly in the slot and inner belt.
(5) The FIR model needs to be improved in the boundary regions of P_1–P_2 and S–P_0 (approximate L ranges: 6.5–7.5 and 2.7–3.0). The prediction error grows sharply in those regions.

In a different study we find that in those boundaries, two other types of inputs are important, namely IMF B_{South} or variables related to dayside magnetic reconnection and its effects (such as magnetic indices); and solar illumination and the resulting changes in ionospheric conductance (Vassiliadis et al., 2004).

Interestingly, the flux in the transition between P_1 and P_2, and in particular at the geosynchronous orbit, is hard to predict using these two fairly general models. Predicting fluxes at the geosynchronous altitude has been attempted several times (e.g., Baker et al., 1990; Koons and Gorney, 1991; O'Brien and McPherron, 2003; Li et al., 2001). As mentioned, the V2002 model (Eq. (1) in this paper) for $L = 6.6$ is identical to the Baker et al. (1990) model, while the Koons and Gorney (1991) neural network is a nonlinear generalization of it (albeit for a geomagnetic input parameter). The nonlinear model by O'Brien and McPherron (2003) is a generalization of Eq. (2) at $L = 6.6$, driven by two geomagnetic inputs.

Probably the most accurate model for the flux at 6.6 currently is the Li et al. (2001) diffusion equation which represents radial transport and losses. The diffusion coefficient is a function of V_{SW} and its fluctuation power. The model is accurate at $L = 6.6$ for long timescales, but has lower accuracy in other regions. We think that the difficulty in the Li et al. model predicting fluxes at $L < 6.6$ is due to the different dynamics in those L shells as reflected in the performance of the FIR and ARMA models. Thus, there is significant potential to improve current capabilities in prediction.

The prediction capability for fluxes in the range $L = 2.7$–3.0 is low due to yet another reason. In addition to geoeffective interplanetary parameters other than V_{SW} being important there, the flux at $L = 2.7$ may contain effects due to the South Atlantic Anomaly. No data preprocessing has been performed specifically for the SAA effect, so the increased error may be a reflection of the flux variability in that region.

4.2. Seasonal variation

The relativistic electron flux varies with season, with average fluxes at equinox being approximately three times as high as at solstices (Baker et al., 1999). The exact causes of the variation are not known, but most probably include a more optimal alignment of the magnetosphere with the heliospheric equatorial plane which modulates fluid instabilities, a Russell–McPherron enhancement of the reconnection rate which increases the "seed" low-energy electron flux, etc. For a discussion of seasonal geomagnetic variations see (Cliver et al., 2000).

Consequently, seasonal variations in $C(L)$ and $e(L)$ are expected. Fig. 5 shows the average correlations in each month for the FIR (5a) and ARMA (5b) models. In the first case, there are peaks at or close to the equinoxes, namely in February, April, and September. Correlations above 60% are observed in the range $L = 4.0$–6.5 while lower correlations are found in P_0 and in $L = 6.5$–9.0.

The ARMA model has lower correlations overall than the FIR model. For $L > 6.6$, correlations abruptly become negative, indicating that the model is not useful at those altitudes. Again, fluxes at the geosynchronous orbit, $L = 6.6$, are most difficult to predict with this model. For lower L values, peaks occur in February–April and August. There is a tendency for the peak correlation to occur later in the year. Below $L = 3.5$, correlations decrease rapidly with L.

Prediction error profiles are similar for both models, and errors are again lower for the FIR model (Fig. 6). A seasonal variation of $e(L)$ is clear in most L shells with lowest errors in equinoxes and highest in solstices. The lowest prediction errors are at $L \simeq 4$, while the highest error values occur in the geosynchronous region, the S–P_0 boundary, and the inner radiation belt.

The interpretation of the seasonal variation is consistent with the solar-cycle-phase analysis: The long-memory FIR model is a better predictor than a short-memory model with or without internal dynamics. Both models predict $j_e(t; L)$ in most of region P_1 and less well in region P_0. This means that the two representations are approximately equivalent there. For the geosynchronous region and larger radial distances, only the FIR model is useful. Both models predict poorly at the geosynchronous orbit and the S–P_0 boundary. The models do well in the slot region and inner belt, where the ARMA model is more accurate.

4.3. Dependence on activity level

Fig. 7a shows the correlation for the FIR model versus the average monthly log-flux. Each test interval is represented by a colored point, where the color coding denotes the L range. Deep blue and purple denote monthly flux levels in the inner belt; green and yellow, levels in P_0 and P_1; and red and orange, levels in P_2. The correlation increases rapidly for $j_e \sim -0.5$ and then slowly above $j_e = 0$. Even for high log-fluxes ($j_e > 3$), however, correlation values are scattered widely.

Fig. 7b shows that the prediction error is clearly correlated with the activity level. As the activity level increases, higher log-flux levels can be predicted at higher accuracy compared to lower ones. Regions P_0 and P_1 are characterized by fairly low prediction errors. The trend is reversed for very low log-flux levels at $j_e < 0$.

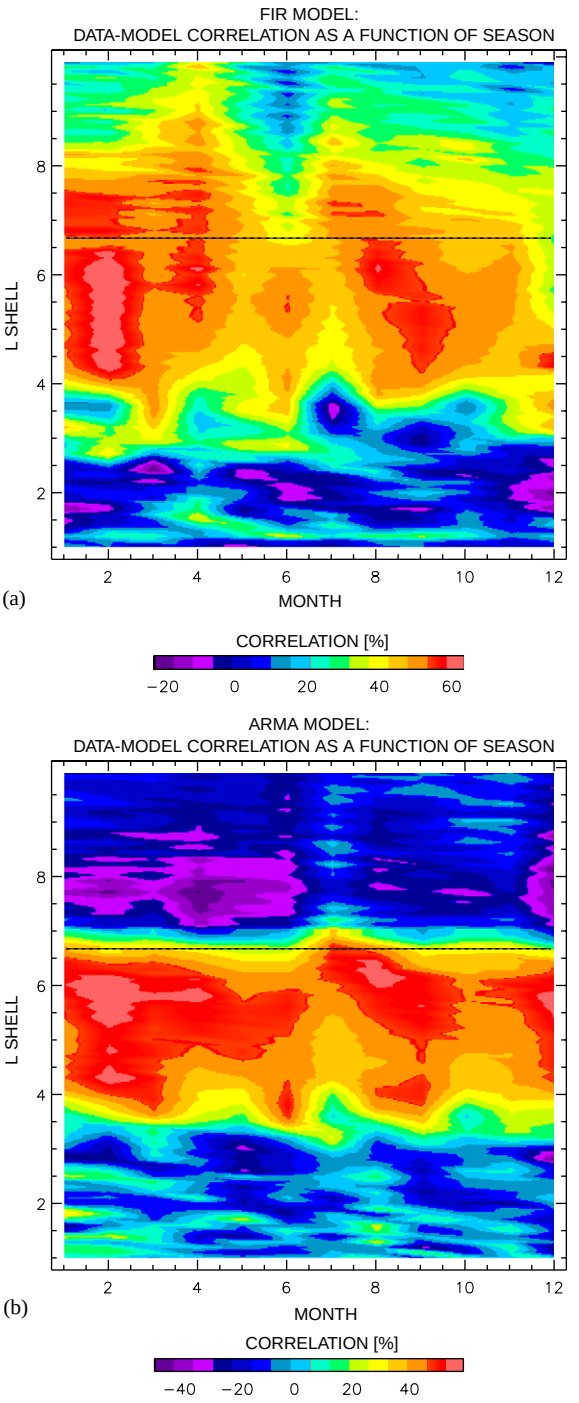

Fig. 5. Seasonal variation of predictability. (a) Data-model correlation of FIR model. Again the test interval length is 1 month. Correlations are averaged over all 9 years. (b) Same as (a) For the ARMA model. The geosynchronous orbit at $L = 6.6$ is marked with a horizontal dashed line.

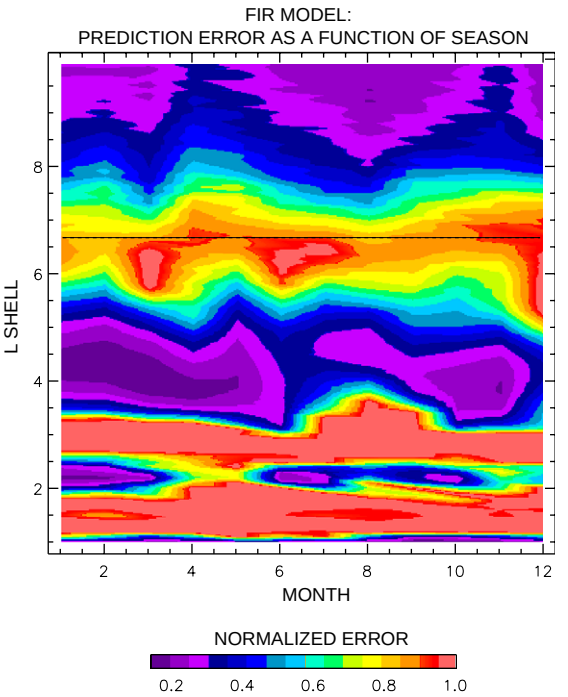

Fig. 6. Seasonal variation: prediction error of the FIR model (cf. Fig. 5).

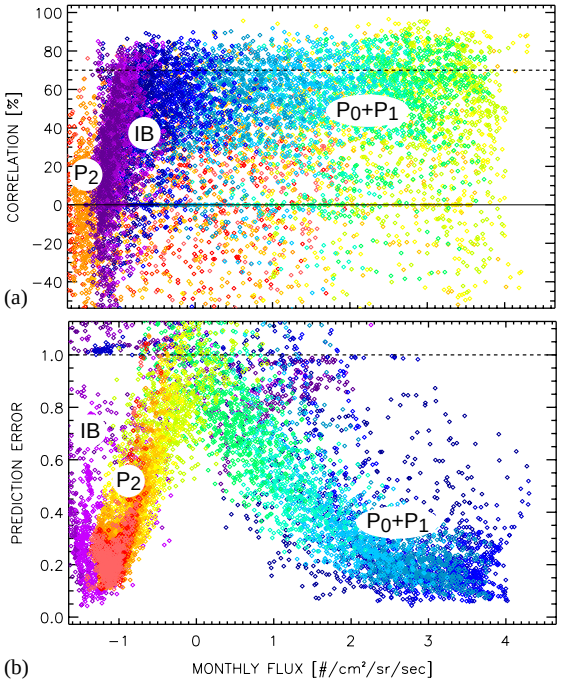

Fig. 7. Prediction capability of the FIR model as a function of monthly activity level. (a) Data-model correlation. The dotted line indicates the correlation $C(L) = 70\%$, corresponding approximately to a prediction efficiency of 50%. Color-coding represents the L parameter value, from the inner belt to region P_2; for details see text. (b) Prediction error. The dotted line indicates the error $e(L) = 1.0$ that a constant-activity model would produce.

5. Summary and discussion

We have examined two dynamic models of the energetic electron flux in the inner magnetosphere developed for CISM. A comparative validation of solar wind–magnetosphere coupling models enables better understanding of this complex interaction and its space weather effects.

Both models use the solar wind velocity V_{SW} as input, but they have fairly different memory times and only one includes dynamical effects of the energetic particle fluxes. Generally the FIR model is the more accurate of the two, which indicates that a memory time of ~ 20 days is useful in forecasting based on V_{SW}. Shorter memory times decrease the prediction capability. A solar wind–magnetosphere coupling based on the velocity is characterized by several day-long timescales (Baker et al., 1990; V2002). The stream structure in the solar wind also produces similar timescales. Reducing the memory time in the model leads to lower predictability. The FIR model is the better model also in region P_2 characterized by low-amplitude quasi-trapped flux. The only exception is at the peak of the solar maximum.

Adding dynamical terms based on the recent history of the flux, $a_i j_e(t-i;L)$, is not typically useful, because of the flux's great variability in time. The ARMA model has better prediction statistics in the slot and inner belt, and during minimum in region P_0.

One should keep in mind that in addition to V_{SW} other interplanetary and magnetospheric variables are important (Vassiliadis et al., 2004). The IMF's Southward component and related magnetospheric quantities constitute one example. Another is solar UV radiation and its effects on ionospheric conductance, which in turn modulates particle losses in the radiation belts.

Both models do poorly at two interesting boundary regions: the geosynchronous orbit and its vicinity, and the boundary S–P_0 between the slot and region P_0. At the geosynchronous orbit, the high prediction error suggests that models of different functional form may be necessary. The IMF B_{South} component is important in that region, possibly because of the role that plasma sheet convection.

In the S–P_0 region, effects of ionospheric heating by UV radiation or Joule heating are important (Vassiliadis et al., 2004). In addition, this region (2.7–3.0) overlaps with the outer plasmasphere, where electron log-flux dynamics are strongly determined by wave-particle interaction (O'Brien and Moldwin, 2003). The situation is made more complicated by the effects of the South Atlantic Anomaly at the vicinity of $L = 2.7$. Therefore

the prediction capability in this range is expected to improve with the inclusion of better log-flux measurements and additional input parameters.

In conclusion, the FIR and ARMA models show how the coupling to one interplanetary variable is implemented and the extent to which it can be used to predict the log-flux in P_0 and P_1. These general dynamic models will be used to make forecasts of space weather conditions as opposed to statistical estimates. Including multiple inputs in these models is expected to reproduce the observed log-flux variations more accurately in radiation belt regions and contribute to the understanding of the electron acceleration and transport mechanisms.

Acknowledgements

We would like to thank S. Fung, X. Shao, P. O'Brien, and D. Boscher for discussions. We are thankful to NASA/NSSDC for providing solar wind data. This material is based upon work supported in part by CISM, which is funded by the STC program of the National Science Foundation under Agreement Number ATM-0120950, and in part by NASA's Living With a Star Program.

References

Baker, D.N., McPherron, R.L., Cayton, T.E., Klebesadel, R.W., 1990. Linear prediction filter analysis of relativistic electron properties at 6.6 R_E. Journal of Geophysical Research 95 (A9), 15133–15140.

Baker, D.N., Pulkkinen, T.I., Li, X., Kanekal, S.G., Ogilvie, K.W., Lepping, R.P., Blake, J.B., Callis, L.B., Rostoker, G., Singer, H.J., Reeves, G.D., 1998. A strong CME-related magnetic cloud interaction with the Earth's magnetosphere: ISTP observations of rapid relativistic electron acceleration on May 15, 1997. Geophysics Research Letter 25 (15), 2975–2978.

Baker, D.N., Kanekal, S.G., Pulkkinen, T.I., Blake, J.B., 1999. Equinoctial and solstitial averages of magnetospheric relativistic electrons: a strong semiannual modulation. Geophysics Research Letter 26 (20), 3193–3196.

Baker, D.N., Weigel, R.S., Rigler, E.J., McPherron, R.L., Vassiladis, D., Arge, C.N., Siscoe, G.L., Spence, H.E., 2004. Sun-to-Magnetosphere Modeling: CISM forecast model development using linked empirical methods. Journal of Atmospheric and Solar-Terrestrial Physics, this issue.

Behnke et al., 1997. The National Space Weather Program: The Implementation Plan, Office of the Federal Coordinator for Meteorological Services and Supporting Research, Washington, DC, FCM-P31-1997.

Blake, J.B., Baker, D.N., Turner, N., Ogilvie, K.W., Lepping, R.P., 1997. Correlation of changes in the outer-zone relativistic-electron population with upstream solar wind and magnetic field measurements. Geophysics Research Letter 24 (8), 927–929.

Boller, B.R., Stolov, H.L., 1970. Kelvin-Helmholtz instability and the semi-annual variation of geomagnetic activity. Journal of Geophysical Research 75, 6073–6084.

Cliver, E.W., Kamide, Y., Ling, A.G., 2000. Mountains versus valleys: Semiannual variation of geomagnetic activity. Journal of Geophysical Research 105 (A2), 2413–2424.

Cook, W.R., Cummings, A.C., Cummings, J.R., Garrard, T.L., Kecman, B., Mewaldt, R.A., Selesnick, R.S., Stone, E.C., Baker, D.N., Von Rosenvinge, T.T., Blake, J.B., Callis, L.B., 1993. PET—A Proton Electron Telescope for studies of magnetospheric, solar, and galactic particles. IEEE Transactions on Geoscience and Remote Sensing 31 (3), 565–571.

Doggett, K. (Ed.), 1996. Proceedings of a Workshop at Boulder, Colorado, June 19–21, 1996. NOAA/SEC, Boulder.

Farrugia, C.J., Gratton, F.T., Torbert, R.B., 2001. Viscous-type processes in the solar wind-magnetosphere interaction. Space Science Review 95 (1–2), 443–456.

Farrugia, C.J., Burlaga, L.F., Jordanova, V.K., Freeman, M.P., Lawrence, G., Matsui, H., Cocheci, C.C., Arnoldy, R.L., Scudder, J.D., Ogilvie, K.W., Lepping, R.P., 2003. Power to the magnetosphere. Advances in Space Research 31 (4), 1117–1122.

Friedel, R.H.W., Reeves, G.D., Obara, T., 2002. Relativistic electron dynamics in the inner magnetosphere—a review. Journal of Atmospheric and Solar-Terrestrial Physics 64 (2), 265–282.

Fung, S.F., Bell, E.V., Tan, L.C., Candey, R.M., Golightly, M.J., Huston, S.J., King, J.H., McGuire, R.E., 2004. Development of a magnetospheric state-based trapped radiation database. Advances in Space Research, in print.

Hudson, M.K., Elkington, S.R., Lyon, J.G., Goodrich, C.C., Rosenberg, T.J., 1999. Simulation of radiation belt dynamics driven by solar wind variations. In: Burch, J.L., Carovillano, R.L., Antiochos, S.K. (Eds.), Sun-Earth Plasma Connections (Geophysical Monograph 109). AGU, Washington, DC.

Koons, H.C., Gorney, D.J., 1991. A neural network model of the relativistic electron flux at geosynchronous orbit. Journal of Geophysical Research 96, 5549–5556.

Koons, H.C., Blake, J.B., Mazur, J., 1999. The impact of the space environment on space systems. TR-99 (1670)-1, Aerospace Corp.

Li, X., Temerin, M., Baker, D.N., Reeves, G.D., Larson, D., 2001. Quantitative prediction of radiation belt electrons at geostationary orbit based on solar wind measurements. Geophysics Research Letter 28 (9), 1887–1890.

O'Brien, T.P., McPherron, R.L., 2003. An empirical dynamic equation for energetic electrons at geosynchronous orbit. Journal of Geophysical Research 108 (A3), 1137 doi:10.1029/2002JA009324.

O'Brien, T.P., Moldwin, M.B., 2003. Empirical plasmapause models from magnetic indices. Geophysics Research Letter 30 (4) Art. No. 1152.

Paulikas, G.A., Blake, J.B., 1979. Effects of the solar wind on magnetospheric dynamics: energetic electrons at the sun-

chronous orbit. In: Olson, W.P. (Ed.), Quantitative Modeling of Magnetospheric Processes (Geophysical Monograph 21). AGU, Washington, DC.

Reeves, G.D., Baker, D.N., Belian, R.D., Blake, J.B., Cayton, T.E., Fennell, J.F., Friedel, R.H.W., Meier, M.M., Selesnick, R.S., Spence, H.E., 1998. The global response of relativistic radiation belt electrons to the January 1997 magnetic cloud. Geophysics Research Letter 25 (17), 3265–3268.

Rigler, E.J., Baker, D.N., Weigel, R.S., Vassiliadis, D., Klimas, A.J., 2004. Adaptive linear prediction of radiation belt electrons using the Kalman filter. Space Weather 2. S03003, doi:10.1029/2003SW000036.

Rostoker, G., Skone, S., Baker, D.N., 1998. On the origin of relativistic electrons in the magnetosphere. Geophysics Research Letter 25, 3701–3704.

Russell, C.T., McPherron, R.L., 1973. Semiannual variation of geomagnetic activity. Journal of Geophysical Research 78 (A7), 92–107.

Vassiliadis, D., 2000. System identification, modeling, and predictions for space weather environments. IEEE Transactions on Plasma Science 28 (6), 1944–1955.

Vassiliadis, D., Klimas, A.J., 1996. Evaluation of nonlinear systems for geomagnetic index forecasting and modeling. Workshop on the Evaluation of Space Weather Forecasts. NOAA/SEC, Boulder, CO, pp. 29–33.

Vassiliadis, D., Klimas, A.J., Kanekal, S.G., Baker, D.N., Weigel, R.S., 2002. Long-term average, solar-cycle, and seasonal response of magnetospheric energetic electrons to the solar wind speed. Journal of Geophysical Research, doi:10.1029/2001JA000506.

Vassiliadis, D., Weigel, R.S., Klimas, A.J., Kanekal, S.G., Mewaldt, R.A., 2003a. Modes of energy transfer between the solar wind and the inner magnetosphere. Physics of Plasmas 10 (2), 463–473.

Vassiliadis, D., Klimas, A.J., Weigel, R.S., Baker, D.N., Rigler, E.J., Kanekal, S.G., Nagai, T., Fung, S.F., Friedel, R.W.H., Cayton, T.E., 2003b. Structure of Earth's outer radiation belt inferred from long-term electron flux dynamics. Geophysics Research Letter 30 (19), 2015 doi:10.1029/2003GL017328..

Vassiliadis, D., Fung, S.F., Klimas, A.J., 2004. Interplanetary and magnetospheric state parameters for the radiation belt electron flux. Journal of Geophysical Research, submitted.